

Spin 3/2 Penta-quarks in anisotropic lattice QCD

N. Ishii¹ *, T. Doi² †, Y. Nemoto³ ‡, M. Oka¹ §, and H. Suganuma⁴ ¶

¹ *Department of Physics, H-27, Tokyo Institute of Technology,
2-12-1 Oh-okayama, Meguro, Tokyo 152-8551, Japan*

² *RIKEN BNL Research Center, Brookhaven National Laboratory, Upton, New York 11973, USA*

³ *Department of Physics, Nagoya University, Furo, Chikusa, Nagoya 464-8602, Japan and*

⁴ *Department of Physics, Kyoto University, Kitashirakawaoiwake, Kyoto 606-8502, Japan*

A high-precision mass measurement for the pentaquark (5Q) Θ^+ in $J^P = 3/2^\pm$ channel is performed in anisotropic quenched lattice QCD using a large number of gauge configurations as $N_{\text{conf}} = 1000$. We employ the standard Wilson gauge action at $\beta = 5.75$ and the $O(a)$ improved Wilson (clover) quark action with $\kappa = 0.1210(0.0010)0.1240$ on a $12^3 \times 96$ lattice with the renormalized anisotropy as $a_s/a_t = 4$. The Rarita-Schwinger formalism is adopted for the interpolating fields. Several types of the interpolating fields with isospin $I = 0$ are examined such as (a) the NK^* -type, (b) the (color-)twisted NK^* -type, (c) a diquark-type. The chiral extrapolation leads to only massive states, i.e., $m_{5Q} \simeq 2.1 - 2.2$ GeV in $J^P = 3/2^-$ channel, and $m_{5Q} = 2.4 - 2.6$ GeV in $J^P = 3/2^+$ channel. The analysis with the hybrid boundary condition(HBC) is performed to investigate whether these states are compact 5Q resonances or not. No low-lying compact 5Q resonance states are found below 2.1GeV.

PACS numbers: 12.38.Gc, 12.39.Mk, 14.20.-c, 14.20.Jn

I. INTRODUCTION

The recent discovery of the manifestly exotic baryon $\Theta^+(1540)$ by the LEPS group at SPring-8 has made a great impact on the exotic hadron physics [1]. Apart from other pentaquark baryon candidates, $\Xi^{--}(1862)$ [2] and $\Theta_c(3099)$ [3], several other candidates of exotic hadrons have also been discovered, such as $X(3872)$, $D_s(2317)$, $S_0(3115)$, $X(3940)$ and $Y(3840)$ [4]. They also receive an increasing interest from theoretical side as well. $\Theta^+(1540)$ is supposed to have baryon number $B = 1$, charge $Q = +1$ and strangeness $S = +1$. Since $uudd\bar{s}$ is the simplest quark content to implement this quantum number, $\Theta^+(1540)$ is a manifestly exotic pentaquark(5Q) state. The penta-quark Θ^+ had been considered several times even before the experimental discovery [5, 6, 7, 8, 9]. In particular, Ref.[5] provided the direct motivation of the experimental search [1]. The discovered peak in the nK^+ invariant mass is centered at 1.54 ± 0.01 GeV with a width smaller than 25 MeV. At the present stage, some groups confirmed the LEPS discovery[10, 11, 12, 13], while the others reported null results[14]. It will still take a while to establish the existence or non-existence of $\Theta^+(1540)$ experimentally [15]. Ref.[12] claims that Θ^+ must be isoscalar, since no Θ^{++} is observed in the pK^+ invariant mass spectrum.

Enormous theoretical efforts have been devoted to 5Q baryons [5, 6, 7, 8, 9, 16, 17, 18, 19, 20, 21, 22, 23, 24, 25, 26, 27, 28, 29, 30, 31, 32, 33, 34, 35, 36, 37, 38, 39,

40, 41, 42, 43, 44, 45, 46, 47, 48, 49, 50, 51, 52, 53, 54]. One of the most challenging problems in understanding its structure is its extremely narrow decay width as $\Gamma \lesssim 1$ MeV [55]. Several ideas have been proposed: (1) $I = 2$ possibility [51], (2) Jaffe-Wilczek's diquark picture [22], (3) πKN hepta-quark picture [29, 56], (4) string picture [40, 41], (5) $J^P = 3/2^-$ possibility [21, 28]. Although each gives a mechanism to explain the narrow decay width, none of them can satisfy all the known properties of $\Theta^+(1540)$ simultaneously.

In this paper, we are interested in the $J = 3/2$ possibility, $J^P = 3/2^-$ in particular. Note that the spin of $\Theta^+(1540)$ has not yet been determined experimentally. In the constituent quark picture, the narrow decay width of $J^P = 3/2^-$ penta-quarks can be understood in the following way [21, 28]. We expect that the special configuration $(0s)^5$ is dominant in the 5Q ground-state in $J^P = 3/2^-$ channel. Although $J^P = 3/2^-$ penta-quarks can decay to KN in the d-wave, the spectroscopic factor to find d-wave KN states in the dominant $(0s)^5$ configuration vanishes. Since the decay is thus allowed only through its sub-dominant d-wave configuration, the decay width is suppressed. Note that it is further suppressed by the d-wave centrifugal barrier, leading to the significantly narrow decay width of $J^P = 3/2^-$ penta-quarks. A possible disadvantage of $J^P = 3/2^-$ assignment is that such a state tends to be massive due to the color-magnetic interaction in the constituent quark models, which seems to be one of the main reasons why there are only a limited number of effective model studies for spin 3/2 penta-quarks [28, 43, 44, 45, 46, 47, 48, 49, 50, 51, 53, 54]. However, it is not clear whether these conventional framework is applicable to a new exotic 5Q system as $\Theta^+(1540)$ without involving any modifications. Indeed, a model was proposed where a part of the role of the color-magnetic

*E-mail : ishii@rarfaxp.riken.jp

†E-mail: doi@quark.phy.bnl.gov

‡E-mail: nemoto@hken.phys.nagoya-u.ac.jp

§E-mail: oka@th.phys.titech.ac.jp

¶E-mail: suganuma@th.phys.titech.ac.jp

interaction can be played by the flavor-spin interaction, which makes the mass-splitting between the $1/2^-$ and the $3/2^-$ states smaller [45].

There have been several lattice QCD calculations of 5Q states by today[57, 58, 59, 60, 61, 62, 63, 64, 65, 66, 67]. However, these studies are restricted to $J^P = 1/2^\pm$ channels except for a very recent one [67]. Enormous efforts are being devoted to more accurate studies of $J^P = 1/2^\pm$ states, using the variational technique to extract multiple excited states, among which a compact resonance state is sought for. Indeed, quite large scale calculations are planned and being performed[68] attempting to elucidate some of the mysterious natures of $\Theta^+(1540)$ such as its diquark structure and/or non-localities desired in interpolating fields. Here, we emphasize again that these studies are aiming at $J^P = 1/2^\pm$ states, not at $3/2^\pm$ states.

In this paper, we present anisotropic lattice QCD results on 5Q states in $J^P = 3/2^\pm$ channels using a large number of gauge configurations as $N_{\text{conf}} = 1000$ as an attempt to search for a low-lying 5Q state in $J^P = 3/2^\pm$ channel. We adopt the standard Wilson gauge action at $\beta = 5.75$ on the $12^3 \times 96$ lattice with the renormalized anisotropy $a_s/a_t = 4$. The anisotropic lattice is known to serve as a powerful tool for high-precision measurements of temporal correlators [69, 70, 71, 72]. The large number of gauge configurations $N_{\text{conf}} = 1000$ plays a key role in our calculation, because 5Q correlators in $J^P = 3/2^\pm$ channels are found to be quite noisy. For quark action, we adopt $O(a)$ -improved Wilson (clover) action with four values of the hopping parameter as $\kappa = 0.1210(0.0010)0.1240$. One of the purpose of our calculation is to examine how the results depend on the choice of interpolating field operators. We employ several types of interpolating fields as (a) the NK^* -type, (b) the (color-)twisted NK^* -type, (c) a diquark-type, and adopt a smeared source to enhance the low-lying spectra.

In $J^P = 3/2^-$ channel, we obtain massive states $m_{5Q} \simeq 2.1 - 2.2$ GeV except for the diquark-type interpolating field, which involves a considerable size of the statistical error. In $J^P = 3/2^+$ channel, we obtain more massive states $m_{5Q} \simeq 2.4 - 2.6$ GeV. None of these 5Q states appear below the NK threshold. Note that the NK threshold is raised up by about 200 – 250 MeV due to the finite extent of the spatial lattice as $L \simeq 2.15$ fm, from which we expect the penta-quark signal to appear below the (raised) NK threshold considering the empirical mass difference between $N+K(1440)$ and $\Theta^+(1540)$. To clarify whether our 5Q states are compact resonance or not, we perform an analysis with the hybrid boundary condition(HBC), which was recently proposed in Ref.[61]. HBC analysis indicates that no compact 5Q resonance is contained in our 5Q states both in $J^P = 3/2^\pm$ channels.

The paper is organized as follows. In Sect. II, we discuss the general formalisms. We begin by introducing several types of interpolating fields, determining their parity transformation properties. We next consider the temporal correlator and its spectral decomposition. We

finally discuss the two-particle scattering states involved in 5Q spectra, and introduce the hybrid boundary condition (HBC) to examine whether a state of our concern is a compact resonance state or not. Sect. III is devoted to the brief descriptions of our lattice action and parameters. In Sect. IV, we present our numerical results for $J^P = 3/2^\pm$ channels in the standard periodic boundary condition(PBC). We show 5Q correlators of various interpolating fields, i.e., the NK^* -type, the (color-)twisted NK^* -type, the diquark-type. In Sect. V, we attempt to determine whether these 5Q states are compact 5Q resonance states or two-particle scattering states by using the HBC. In Sect. VI, we summarize our results.

II. GENERAL FORMALISMS

A. Interpolating fields

We consider an iso-scalar interpolating field of NK^* -type in Rarita-Schwinger form [73, 74, 75] as

$$\begin{aligned} \psi_\mu \equiv & \epsilon_{abc} (u_a^T C \gamma_5 d_b) u_c \cdot (\bar{s}_d \gamma_\mu d_d) \\ & - \epsilon_{abc} (u_a^T C \gamma_5 d_b) d_c \cdot (\bar{s}_d \gamma_\mu u_d), \end{aligned} \quad (1)$$

where μ denotes the Lorentz index, $a-d$ refer to the color indices, and $C = \gamma_4 \gamma_2$ denotes the charge conjugation matrix. Unless otherwise indicated, the gamma matrices are represented in the Euclidean form given in Ref.[76].

We are also interested in the (color-)twisted NK^* -type interpolating field as

$$\begin{aligned} \psi_\mu \equiv & \epsilon_{abc} (u_a^T C \gamma_5 d_b) u_d \cdot (\bar{s}_d \gamma_\mu d_c) \\ & - \epsilon_{abc} (u_a^T C \gamma_5 d_b) d_d \cdot (\bar{s}_d \gamma_\mu u_c), \end{aligned} \quad (2)$$

which is an extension to the one originally proposed in Ref.[57] to study $J^P = 1/2^P$ 5Q states. It has a slightly more elaborate color-structure than Eq. (1), suggesting somewhat stronger coupling to a genuine 5Q state, if it exists, than simple NK^* states.

Another interpolating fields of our possible interests are diquark-type interpolating fields such as

$$\psi_\mu \equiv \epsilon_{abc} \epsilon_{def} \epsilon_{cfg} (u_a^T C \gamma_5 d_b) (u_d^T C \gamma_5 \gamma_\mu d_e) C \gamma_5 \bar{s}_g \quad (3)$$

which is an extension to the one proposed in Refs. [36, 58]. The first factor corresponds to the scalar diquark (color $\mathbf{\bar{3}}$, $I = 0$, $J^P = 0^+$), which is expected to play important roles in hadron physics [77]. The second factor corresponds to the vector diquark (color $\mathbf{\bar{3}}$, $I = 0$, $J^P = 1^-$). Note that, although the axial-vector diquark (color $\mathbf{\bar{3}}$, $I = 1$, $J^P = 1^+$) is considered to play a more important role than the vector diquark, it cannot replace the vector diquark due to its iso-vector nature. Unless otherwise indicated, we refer to Eq. (3) as the “*diquark-type*” interpolating field. We can also consider another interpolating field of diquark-type as

$$\psi_\mu \equiv \epsilon_{abc} \epsilon_{def} \epsilon_{cfg} (u_a^T C d_b) (u_d^T C \gamma_5 \gamma_\mu d_e) C \bar{s}_g, \quad (4)$$

which consists of the pseudo-scalar diquark (color $\bar{3}$, $I = 0$, $J^P = 0^-$) and the vector diquark. However, actual lattice QCD calculation shows that its correlator is afflicted with quite a huge statistical error. A possible reason could be attributed to the fact that both of these diquark fields do not survive the non-relativistic limit. Hence, we do not consider this interpolating field in this paper.

Under the spatial reflection of the quark fields as

$$q(\tau, \vec{x}) \rightarrow \gamma_4 q(\tau, -\vec{x}), \quad (5)$$

all of these interpolating fields transform as

$$\psi_i(\tau, \vec{x}) \rightarrow -\gamma_4 \psi_i(\tau, -\vec{x}), \quad (6)$$

for $i = 1, 2, 3$.

B. 5Q correlators and parity projection

We consider the Euclidean temporal correlator as

$$G_{\mu\nu}(\tau) \equiv \sum_{\vec{x}} \langle \psi_\mu(\tau, \vec{x}) \bar{\psi}_\nu(0, \vec{0}) \rangle, \quad (7)$$

where $\sum_{\vec{x}}$ projects the total 5Q momentum to zero. Since the spin 3/2 contribution from the temporal component of Rarita-Schwinger spinor vanishes in the rest frame, we can restrict ourselves to the spatial parts, i.e., $\mu\nu = 1, 2, 3$. Now, Eq. (7) is decomposed in the following way:

$$G_{ij}(\tau) = \mathbf{P}_{ij}^{(3/2)} G^{(3/2)}(\tau) + \mathbf{P}_{ij}^{(1/2)} G^{(1/2)}(\tau), \quad (8)$$

where $i, j = 1, 2, 3$ denote the spatial part of the Lorentz indices, $\mathbf{P}^{(3/2)}$ and $\mathbf{P}^{(1/2)}$ denote the projection matrices onto the spin 3/2 and 1/2 subspaces defined as

$$\begin{aligned} \mathbf{P}_{ij}^{(3/2)} &\equiv \delta_{ij} - (1/3)\gamma_i\gamma_j, \\ \mathbf{P}_{ij}^{(1/2)} &\equiv (1/3)\gamma_i\gamma_j. \end{aligned} \quad (9)$$

They satisfy the following relations as

$$\begin{aligned} \mathbf{P}_{ij}^{(3/2)} \mathbf{P}_{jk}^{(3/2)} &= \mathbf{P}_{ik}^{(3/2)} \\ \mathbf{P}_{ij}^{(1/2)} \mathbf{P}_{jk}^{(1/2)} &= \mathbf{P}_{ik}^{(1/2)} \\ \mathbf{P}_{ij}^{(1/2)} + \mathbf{P}_{ij}^{(3/2)} &= \delta_{ij} \\ \mathbf{P}_{ij}^{(1/2)} \mathbf{P}_{jk}^{(3/2)} &= \mathbf{P}_{ij}^{(3/2)} \mathbf{P}_{jk}^{(1/2)} = 0. \end{aligned} \quad (10)$$

Here, summations over repeated indices are understood. $G^{(3/2)}(\tau)$ and $G^{(1/2)}(\tau)$ in Eq. (7) denote the spin 3/2 and 1/2 contributions to $G(\tau)$, respectively, which can be derived by operating $\mathbf{P}^{(3/2)}$ and $\mathbf{P}^{(1/2)}$ on $G(\tau)$, respectively. (In our practical lattice QCD calculation, we construct the Rarita-Schwinger correlator $G_{ij}(\tau)$ for $i = 1, 2, 3$ and $j = 3$ (fixed), and multiply $\mathbf{P}^{(3/2)}$ from the left to obtain $G^{(3/2)}(\tau)$.)

In the asymptotic region ($0 \ll \tau \ll N_t$), contaminations of excited states are suppressed. Considering the parity transformation property Eq. (6), $G^{(3/2)}(\tau)$ and $G^{(1/2)}(\tau)$ are expressed in this region as

$$\begin{aligned} G^{(3/2)}(\tau) &= P_+ \left\{ |\lambda_{3/2^-}|^2 e^{-\tau m_{3/2^-}} + |\lambda_{3/2^+}|^2 e^{-(N_t - \tau) m_{3/2^+}} \right\} \\ &\quad - P_- \left\{ |\lambda_{3/2^+}|^2 e^{-\tau m_{3/2^+}} + |\lambda_{3/2^-}|^2 e^{-(N_t - \tau) m_{3/2^-}} \right\} \\ G^{(1/2)}(\tau) &= P_+ \left\{ |\lambda_{1/2^-}|^2 e^{-\tau m_{1/2^-}} + |\lambda_{1/2^+}|^2 e^{-(N_t - \tau) m_{1/2^+}} \right\} \\ &\quad - P_- \left\{ |\lambda_{1/2^+}|^2 e^{-\tau m_{1/2^+}} + |\lambda_{1/2^-}|^2 e^{-(N_t - \tau) m_{1/2^-}} \right\}, \end{aligned} \quad (11)$$

where $P_\pm \equiv (1 \pm \gamma_4)/2$ denote the projection matrices onto the ‘‘upper’’ and ‘‘lower’’ Dirac subspaces, respectively. $m_{3/2^\pm}$ and $m_{1/2^\pm}$ denote the lowest-lying masses in $J^P = 3/2^\pm$ and $1/2^\pm$ channels, respectively. $\lambda_{3/2^\pm}$ and $\lambda_{1/2^\pm}$ represent the couplings to the interpolating field Eq. (1) with $J^P = 3/2^\pm$ and $1/2^\pm$ states, respectively. In Eq. (11), we adopt the anti-periodic boundary condition along the temporal direction. A brief derivation of Eq. (8) and Eq. (11) is presented in Appendix. A. The forward propagation is dominant in the region $0 < \tau \lesssim N_t/2$, while the backward propagation is dominant in the region $N_t/2 \lesssim \tau < N_t$. To separate the negative (positive) parity contribution, we restrict ourselves to the region $0 < \tau \lesssim N_t/2$, and examine the ‘‘upper’’ (‘‘lower’’) Dirac component.

C. Scattering states involved in 5Q spectrum

We consider the (two-particle) scattering states involved in 5Q spectrum. For $J^P = 3/2^\pm$ iso-scalar pentaquarks, NK and NK* scattering states play an important role. (ΔK does not couple to the iso-scalar channel.) These states are expressed as

$$|N(\vec{p}, s)K(-\vec{p})\rangle, \quad |N(\vec{p}, s)K^*(-\vec{p}, i)\rangle, \quad (12)$$

where s and i denote the spin of the nucleon and K^* , and \vec{p} denotes the spatial momentum allowed for a particular choice of the spatial boundary condition adopted. For instance, if these hadrons are subject to the spatially periodic boundary condition, their momenta are quantized as

$$p_i = 2n_i\pi/L, \quad n_i \in \mathbf{Z}, \quad (13)$$

where L denotes the spatial extent of the lattice. In contrast, if they are subject to the spatially anti-periodic boundary condition, their momenta are quantized as

$$p_i = (2n_i + 1)\pi/L, \quad n_i \in \mathbf{Z}. \quad (14)$$

κ		0.1210	0.1220	0.1230	0.1240	emp.
NK*(s-wave)	PBC	2.996	2.815	2.633	2.445	1.830
NK*(p-wave)	PBC	3.222	3.052	2.883	2.710	2.163
NK(p/d-wave)	PBC	2.987	2.806	2.624	2.438	1.865
NK*(s/p-wave)	HBC	3.167	2.995	2.823	2.647	2.084
NK(p/d-wave)	HBC	2.924	2.739	2.553	2.363	1.770

TABLE I: Numerical values of NK and NK* thresholds for each hopping parameter κ in the physical unit GeV in the spatial lattice of the size $L \simeq 2.15$ fm in PBC and HBC. The rightmost column labeled as ‘‘emp.’’ shows the thresholds for the physical values of N, K, and K* as $m_N \simeq 0.94$ GeV, $m_K \simeq 0.5$ GeV, $m_{K^*} \simeq 0.89$ GeV.

We first perform the parity projections. The positive and the negative parity states are obtained in the following way:

$$|NK(\pm)\rangle \quad (15)$$

$$= |N(\vec{p}, s)K(-\vec{p})\rangle \mp |N(-\vec{p}, s)K(\vec{p})\rangle$$

$$|NK^*(\pm)\rangle \quad (16)$$

$$= |N(\vec{p}, s)K^*(-\vec{p}, i)\rangle \mp |N(-\vec{p}, s)K^*(\vec{p}, i)\rangle.$$

Assuming that the interactions between N and K and between N and K* are weak, their energies are approximated as

$$E_{NK} \simeq \sqrt{m_N^2 + \vec{p}^2} + \sqrt{m_K^2 + \vec{p}^2} \quad (17)$$

$$E_{NK^*} \simeq \sqrt{m_N^2 + \vec{p}^2} + \sqrt{m_{K^*}^2 + \vec{p}^2}, \quad (18)$$

respectively. The scattering states which couple to $J^P = 3/2^\pm$ penta-quarks are obtained as spin-3/2 projections of Eq. (15) and Eq. (16). The d-wave NK states and the s-wave NK* states can couple to the $J^P = 3/2^-$ channel, while the p-wave NK states and NK* states can couple to the $J^P = 3/2^+$ channel.

The scattering states with vanishing spatial momentum $\vec{p} = \vec{0}$ are exceptional in the following sense. On the one hand, the positive parity states vanish, because the first terms coincides with the second terms in Eq. (15) and Eq. (16) in the right hand side. On the other hand, the negative parity states are constructed only from the spin degrees of freedom, i.e., the spin degrees of freedom of the nucleon in Eq. (15), and the spin degrees of freedoms of the nucleon and K* in Eq. (16). By counting the degeneracy of the resulting states, it is straightforward to see that no d-wave states are contained, i.e., Eq. (15) gives only s-wave NK states in $J^P = 1/2^-$ channel, and that Eq. (16) gives only s-wave NK* states in $J^P = 1/2^-$ and $3/2^-$ channels.

D. Hybrid boundary condition(HBC)

In order to determine whether a state of our concern is a compact 5Q resonance state or a scattering state

of two particles, we use two distinct spatial boundary conditions(BC), i.e., the (standard) periodic BC(PBC) and the hybrid BC(HBC), which is recently proposed in Ref.[61]. In PBC, one imposes the spatially periodic BC on u,d and s-quarks. As a result, all the hadrons are subject to the periodic BC. In this case, due to Eq. (13), all hadrons can take zero-momentum, and the smallest non-vanishing momentum \vec{p}_{\min} is of the form as

$$(\pm 2\pi/L, 0, 0), \quad (0, \pm 2\pi/L, 0), \quad (0, 0, \pm 2\pi/L), \quad (19)$$

which gives

$$|\vec{p}_{\min}^{\text{PBC}}| = 2\pi/L. \quad (20)$$

On the other hand, in HBC, we impose the spatially anti-periodic BC on u and d-quarks, whereas the spatially periodic BC is imposed on s-quark. Since $N(uud, udd)$, $K(u\bar{s}, d\bar{s})$ and $K^*(u\bar{s}, d\bar{s})$ contain odd numbers of u and d quarks, they are subject to the anti-periodic BC. Therefore, due to Eq. (14), N, K and K* cannot have a vanishing momentum in HBC. The smallest possible momentum \vec{p}_{\min} is of the form as

$$(\pm\pi/L, \pm\pi/L, \pm\pi/L). \quad (21)$$

Hence, its norm $|\vec{p}_{\min}|$ is expressed as

$$|\vec{p}_{\min}^{\text{HBC}}| = \sqrt{3}\pi/L. \quad (22)$$

In contrast, $\Theta^+(uudd\bar{s})$ is subject to the spatially periodic BC, since it contains even number of u and d quarks. Therefore, Θ^+ can have the vanishing momentum.

Switching from PBC, HBC affects the low-lying two-particle scattering spectrum. A drastic change is expected in the s-wave NK* channel. In PBC, the energy of the lowest NK* state is given as

$$E_{\min}^{\text{PBC}}(NK^*(\text{s-wave})) \simeq m_N + m_{K^*}. \quad (23)$$

In contrast, in HBC, since both N and K* are required to have non-vanishing momenta $|\vec{p}_{\min}| = \sqrt{3}\pi/L$, the energy of the lowest NK* state is raised up as

$$E_{\min}^{\text{HBC}}(NK^*(\text{s-wave})) \quad (24)$$

$$\simeq \sqrt{m_N^2 + 3\pi^2/L^2} + \sqrt{m_{K^*}^2 + 3\pi^2/L^2}.$$

Note that the shift amounts typically to a few hundred MeV for $L \sim 2$ fm.

HBC affects NK(d-wave), NK(p-wave), NK*(p-wave) as well. However, these changes are not as drastic as that in NK*(s-wave), because they are induced by the minor change in the minimum momentum from $|\vec{p}_{\min}| = 2\pi/L$ to $\sqrt{3}\pi/L$. In PBC, the energies of the lowest two-particles states are expressed as

$$E_{\min}^{\text{PBC}}(NK(\text{p/d-wave})) \quad (25)$$

$$\simeq \sqrt{m_N^2 + 4\pi^2/L^2} + \sqrt{m_K^2 + 4\pi^2/L^2}$$

$$E_{\min}^{\text{PBC}}(NK^*(\text{p-wave}))$$

$$\simeq \sqrt{m_N^2 + 4\pi^2/L^2} + \sqrt{m_{K^*}^2 + 4\pi^2/L^2}.$$

In HBC, they are shifted down as

$$\begin{aligned}
E_{\min}^{\text{HBC}}(NK(\text{p/d-wave})) & \quad (26) \\
& \simeq \sqrt{m_N^2 + 3\pi^2/L^2} + \sqrt{m_K^2 + 3\pi^2/L^2} \\
E_{\min}^{\text{HBC}}(NK^*(\text{p-wave})) & \\
& \simeq \sqrt{m_N^2 + 3\pi^2/L^2} + \sqrt{m_{K^*}^2 + 3\pi^2/L^2}.
\end{aligned}$$

Numerical values of NK and NK* thresholds for each hopping parameter in spatial lattice of the size $L \simeq 2.15$ fm for both PBC and HBC are summarized in Table I.

In contrast to the scattering states, HBC is not expected to affect a compact 5Q resonance Θ^+ so much. Since $\Theta^+(uudd\bar{s})$ can have vanishing momentum also in HBC, the shift of the penta-quark mass m_{5Q} originates only from the change in its intrinsic structure. In this case, the shift is expected to be less significant than the shift induced by the kinematic reason as is the case in N, K, and K*. Now our way to find a compact 5Q resonance state is to seek for such a state which is not affected by HBC.

III. LATTICE ACTIONS AND PARAMETERS

To generate gauge field configurations, we use the standard plaquette action on the anisotropic lattice of the size $12^3 \times 96$ as

$$\begin{aligned}
S_G &= \frac{\beta}{N_c} \frac{1}{\gamma_G} \sum_{x, i < j \leq 3} \text{ReTr} \{1 - P_{ij}(x)\} \quad (27) \\
&+ \frac{\beta}{N_c} \gamma_G \sum_{x, i \leq 3} \text{ReTr} \{1 - P_{i4}(x)\},
\end{aligned}$$

where $P_{\mu\nu}(x) \in \text{SU}(3)$ denotes the plaquette operator in the μ - ν -plane. The lattice parameter and the bare anisotropy parameter are fixed as $\beta \equiv 2N_c/g^2 = 5.75$ and $\gamma_G = 3.2552$, respectively. These values are determined to reproduce the renormalized anisotropy as $\xi \equiv a_s/a_t = 4$ [69]. Adopting the pseudo-heat-bath algorithm, we pick up gauge field configurations every 500 sweeps after skipping 10,000 sweeps for the thermalization. We use totally 1000 gauge field configurations to construct the temporal correlators. Note that the high statistics of $N_{\text{conf}} = 1000$ is quite essential for our study, because the 5Q correlators for spin 3/2 states are found to be rather noisy. In fact, a preliminary analysis with less statistics $N_{\text{conf}} \simeq 500$ leads to a spurious resonance-like state [78]. The lattice spacing is determined from the static quark potential adopting the Sommer parameter $r_0^{-1} = 395$ MeV ($r_0 \sim 0.5$ fm) as $a_s^{-1} = 1.100(6)$ GeV ($a_s \simeq 0.18$ fm). Note that the lattice size $12^3 \times 96$ amounts to $(2.15\text{fm})^3 \times (4.30\text{fm})$ in the physical unit.

We adopt the $O(a)$ -improved Wilson (clover) action on

the anisotropic lattice for quark fields ψ and $\bar{\psi}$ as [70]

$$\begin{aligned}
S_F &\equiv \sum_{x,y} \bar{\psi}(x) K(x,y) \psi(y), \quad (28) \\
K(x,y) &\equiv \delta_{x,y} - \kappa_t \left\{ (1 - \gamma_4) U_4(x) \delta_{x+\hat{4},y} \right. \\
&\quad \left. + (1 + \gamma_4) U_4^\dagger(x - \hat{4}) \delta_{x-\hat{4},y} \right\} \\
&- \kappa_s \sum_i \left\{ (r - \gamma_i) U_i(x) \delta_{x+\hat{i},y} \right. \\
&\quad \left. + (r + \gamma_i) U_i^\dagger(x - \hat{i}) \delta_{x-\hat{i},y} \right\} \\
&- \kappa_s c_E \sum_i \sigma_{i4} F_{i4} \delta_{x,y} - r \kappa_s c_B \sum_{i < j} \sigma_{ij} F_{ij} \delta_{x,y},
\end{aligned}$$

where κ_s and κ_t denote the hopping parameters for the spatial and the temporal directions, respectively. The field strength $F_{\mu\nu}$ is defined through the standard clover-leaf-type construction. r denotes the Wilson parameter. c_E and c_B denote the clover coefficients. To achieve the tadpole improvement, the link variables are rescaled as $U_i(x) \rightarrow U_i(x)/u_s$ and $U_4(x) \rightarrow U_4(x)/u_t$, where u_s and u_t denote the mean-field values of the spatial and temporal link variables, respectively [70, 71]. This is equivalent to the redefinition of the hopping parameters as the tadpole-improved ones (with tilde), i.e., $\kappa_s = \tilde{\kappa}_s/u_s$ and $\kappa_t = \tilde{\kappa}_t/u_t$. The anisotropy parameter is defined as $\gamma_F \equiv \tilde{\kappa}_t/\tilde{\kappa}_s$, which coincides with the renormalized anisotropy $\xi = a_s/a_t$ for sufficiently small quark mass at the tadpole-improved level [70]. For given κ_s , the four parameters r , c_E , c_B and κ_s/κ_t should be, in principle, tuned so that ‘‘Lorentz symmetry’’ holds up to discretization errors of $O(a^2)$. Here, r , c_E and c_B are fixed by adopting the tadpole improved tree-level values as

$$r = \frac{1}{\xi}, \quad c_E = \frac{1}{u_s u_t^2}, \quad c_B = \frac{1}{u_s^3}. \quad (29)$$

Only the value of $\kappa_s/\kappa_t (= \gamma_F \cdot (u_s/u_t))$ is tuned nonperturbatively by using the meson dispersion relation [70]. It is convenient to define κ as

$$\frac{1}{\kappa} \equiv \frac{1}{\tilde{\kappa}_s} - 2(\gamma_F - 3r - 4). \quad (30)$$

Then the bare quark mass is expressed as $m_0 = \frac{1}{2}(1/\kappa - 8)$ in the spatial lattice unit in the continuum limit. This κ plays the role of the hopping parameter ‘‘ κ ’’ in the isotropic formulation. For detail, see Refs. [70, 71], where we take the lattice parameters. The values of the lattice parameters are summarized in Table II.

We adopt four values of the hopping parameter as $\kappa = 0.1210, 0.1220, 0.1230$ and 0.1240 , which correspond to $m_\pi/m_\rho = 0.81, 0.78, 0.73$ and 0.66 , respectively. These values roughly cover the region $m_s \lesssim m \lesssim 2m_s$. For temporal direction, we impose anti-periodic boundary condition on all the quark fields. For spatial directions, we impose periodic boundary condition on all the quarks, unless otherwise indicated. We refer to this boundary condition as ‘‘periodic BC (PBC)’’.

β	γ_G	a_s/a_t	a_s^{-1} [GeV]	Size	N_{conf}	u_s	u_t	γ_F	κ_c	Values of κ
5.75	3.2552	4	1.100(6)	$12^3 \times 96$	1000	0.7620(2)	0.9871(0)	3.909	0.12640(5)	0.1240, 0.1230, 0.1220, 0.1210

TABLE II: Parameters of the lattice simulation. The spatial lattice spacing a_σ is determined with $r_0^{-1} = 385$ MeV for the Sommer parameter. The mean-field values of link variables (u_σ and u_τ) are defined in the Landau gauge. κ_c denotes the critical value of κ .

κ	0.1210	0.1220	0.1230	0.1240	$\kappa_{\text{phys.}}$
m_π	1.007(2)	0.897(1)	0.785(2)	0.658(2)	0.140
m_ρ	1.240(4)	1.157(5)	1.074(7)	0.991(11)	0.823(13)
m_K	0.846(2)	0.785(1)	0.722(2)	0.658(2)	0.476(2)
m_{K^*}	1.119(6)	1.076(7)	1.033(9)	0.991(11)	0.902(15)
m_N	1.877(4)	1.739(3)	1.600(4)	1.454(5)	1.164(8)
m_{N^*}	2.325(17)	2.194(21)	2.059(28)	1.918(42)	1.648(53)

TABLE III: Masses of π , ρ , K , K^* , N , and N^* for each hopping parameter κ in the physical unit GeV. $\kappa_{\text{phys.}} \simeq 0.1261$ denotes the value of κ which achieves $m_\pi \simeq 0.14$ GeV.

By keeping $\kappa_s = 0.1240$ fixed for s quark, and by changing $\kappa = 0.1210 - 0.1240$ for u and d quarks, we perform the chiral extrapolation to the physical quark mass region. In the following part of the paper, we will use

$$(\kappa_s, \kappa) = (0.1240, 0.1220), \quad (31)$$

as a typical set of hopping parameters in presenting correlators and effective mass plots. For convenience, we summarize masses of π , ρ , K , K^* , N and N^* ($J^P = 1/2^-$ baryon) for each hopping parameter κ together with their values at the physical quark mass in Table III. Here, the chiral extrapolations of these particles are performed by a linear function in m_π^2 . Unless otherwise indicated, we adopt the jackknife prescription to estimate the statistical errors.

We use a smeared source to enhance the low-lying spectra. More precisely, we employ spatially extended interpolating fields of the gaussian size $\rho \simeq 0.4$ fm, which is obtained by replacing the quark fields $q(x)$ in 5Q interpolating fields by the smeared quark fields $q_{\text{smeared}}(x)$ in the Coulomb gauge as

$$q_{\text{smeared}}(\tau, \vec{x}) \equiv \mathcal{N} \sum_{\vec{y}} \exp\left\{-\frac{|\vec{x} - \vec{y}|^2}{2\rho^2}\right\} q(\tau, \vec{y}), \quad (32)$$

where \mathcal{N} is an appropriate normalization factor. For a practical use, we extend Eq. (32) appropriately so as to fit a particular choice of the spatial boundary condition. In this paper, we present correlators with a smeared source and a point sink.

IV. NUMERICAL RESULTS ON 5Q SPECTRUM

We present our lattice QCD results on 5Q spectrum in the standard periodic boundary condition(PBC) in this

section.

A. $J^P = 3/2^-$ 5Q spectrum in PBC

We consider 5Q spectrum in $J^P = 3/2^-$ channel. In Fig. 1, we show the effective mass plots in $J^P = 3/2^-$ channel for three interpolating fields, i.e., (a) the NK^* -type, (b) the twisted NK^* -type, (c) a diquark-type. The dotted lines indicate the s-wave NK^* and the d-wave NK thresholds, which happen to coincide accidentally in Fig. 1 for the spatial lattice size $L \simeq 2.15$ fm.

We define the effective mass as a function of τ by

$$m_{\text{eff}}(\tau) \equiv \log\left(\frac{G^{(3/2)}(\tau)}{G^{(3/2)}(\tau+1)}\right), \quad (33)$$

where $G^{(3/2)}(\tau)$ denotes the temporal correlator. At sufficiently large τ , the correlator is dominated by the lowest-lying state with energy m as $G^{(3/2)}(\tau) \sim Ae^{-m\tau}$. Then Eq. (33) gives a constant as $m_{\text{eff}}(\tau) \simeq m$. Thus a plateau in $m_{\text{eff}}(\tau)$ indicates that the correlator is saturated by a single-state. In such cases, we can perform a single-exponential fit in the plateau region.

Fig. 1 (a) shows the effective mass plot for the NK^* -type interpolating field. In the region $0 \leq \tau \leq 24$, the contamination of the higher spectral contributions are gradually reduced, which is indicated by the decreases in $m_{\text{eff}}(\tau)$. There is a plateau in the interval $25 \lesssim \tau \lesssim 35$, where a single-state is expected to dominate the 5Q correlator. Beyond $\tau \sim 36$, the statistical error becomes large. In addition, the effect of the backward propagation becomes gradually more significant as $\tau \sim 48$ is approached. Hence, we simply neglect the data for $\tau \gtrsim 36$, and perform the single-exponential fit in the region $25 \leq \tau \leq 35$. We obtain $m_{5Q} = 2.90(2)$ GeV, which is denoted by the solid line. One sees that the 5Q states appears above the s-wave NK^* and the d-wave NK thresholds.

Fig. 1 (b) shows the effective mass plot for the twisted NK^* -type interpolating field. There is a plateau in the interval $24 \lesssim \tau \lesssim 35$, where the single-exponential fit is performed leading to $m_{5Q} = 2.89(1)$ GeV. The 5Q state is again above the s-wave NK^* and the d-wave NK thresholds.

Fig. 1 (c) shows the effective mass plot for the diquark-type interpolating field. We see that the statistical error is too large to identify the plateau unambiguously. Hence, we do not perform the fit. Note that this plot is obtained by using $N_{\text{conf}} = 1000$ gauge configurations. A

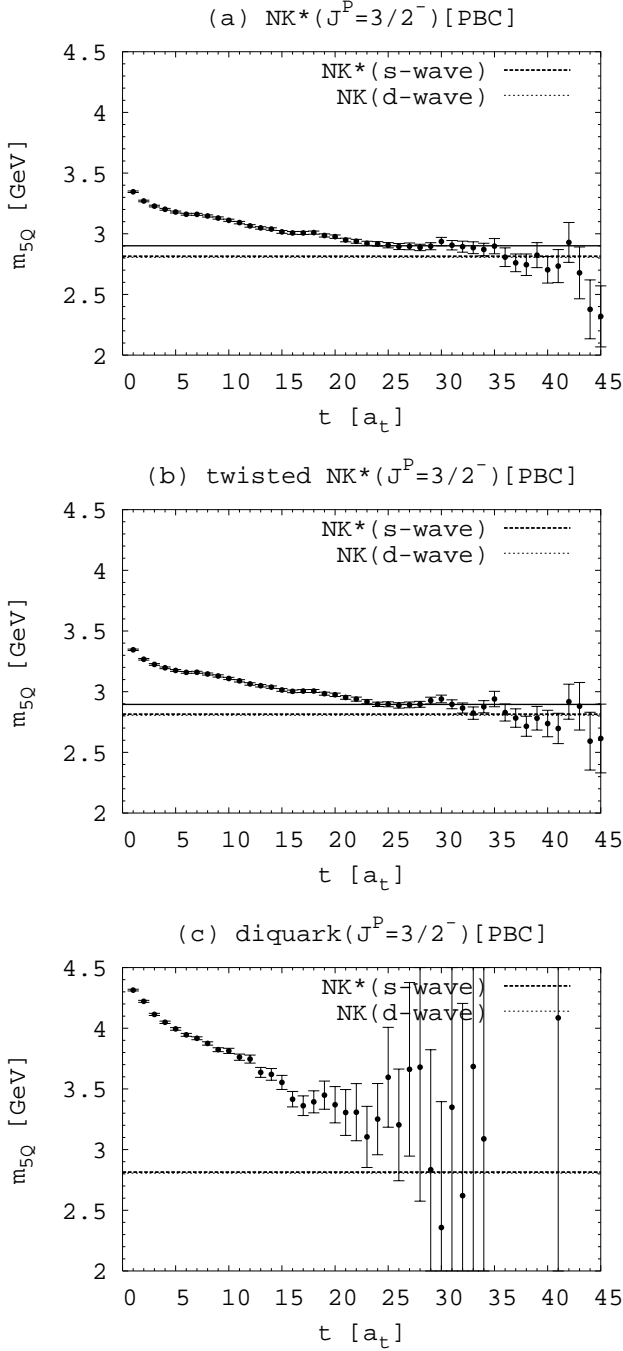


FIG. 1: The 5Q effective mass plots in $J^P = 3/2^-$ channel in the standard periodic BC(PBC) for three types of interpolating fields, i.e., (a) the NK^* -type, (b) the twisted NK^* -type, and (c) the diquark-type. Eq. (31) is adopted as a typical set of hopping parameters. The statistical error is estimated with the jackknife prescription. The dotted lines indicate the s-wave NK^* and the d-wave NK threshold in the spatial lattice size $L \simeq 2.15$ fm. Note that they accidentally coincide with each other. The solid lines denote the results of the single-exponential fit performed in each plateau region.

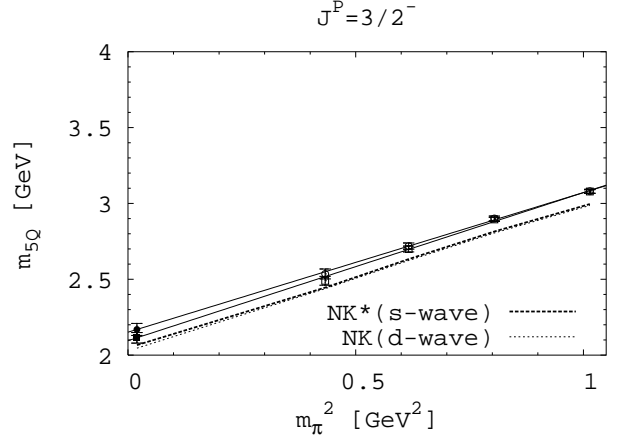


FIG. 2: m_{5Q} in $J^P = 3/2^-$ channel against m_π^2 for the two interpolating fields, i.e., (circle) the NK^* -type, (box) the twisted NK^* -type. Open symbols denote the direct lattice QCD data, while the closed symbols and the solid lines represent the results of the chiral extrapolations to the physical quark mass region.

J^P	I.F.	0.1210	0.1220	0.1230	0.1240	$\kappa_{\text{phys.}}$
$3/2^-$	(a)	3.08(1)	2.90(2)	2.72(2)	2.54(3)	2.17(4)
$3/2^-$	(b)	3.08(1)	2.89(1)	2.70(2)	2.49(3)	2.11(4)
$3/2^-$	(c)	—	—	—	—	—
$3/2^+$	(a)	3.52(2)	3.34(3)	3.17(11)	3.00(5)	2.64(7)
$3/2^+$	(b)	3.27(3)	3.11(4)	2.95(5)	2.83(9)	2.48(10)
$3/2^+$	(c)	3.34(2)	3.16(2)	2.98(3)	2.78(5)	2.42(6)

TABLE IV: m_{5Q} for each value of κ in the physical unit GeV. The first column labeled by “ J^P ” indicates the spin and the parity. The second column labeled by “I.F.” indicates the interpolating field used, i.e., (a) the NK^* -type, (b) the twisted NK^* -type, (c) the diquark-type. $\kappa_{\text{phys.}} \simeq 0.1261$ denotes the value of κ which achieve $m_\pi \simeq 0.14$ GeV. “—” indicates that the fitting is not performed due to the large statistical error.

possible reason for such a large noise is that the interpolating field Eq. (3) does not survive the non-relativistic limit due to the vector diquark.

Now, we perform the chiral extrapolation. As mentioned before, we keep $\kappa = 0.1240$ fixed for s-quark, and vary $\kappa = 0.1210-0.1240$ for u and d quarks. Fig. 2 shows the 5Q masses in $J^P = 3/2^-$ channel against m_π^2 . Circles and boxes denote the data obtained from the NK^* -type and the twisted NK^* -type 5Q correlators, respectively. Note that they agree with each other within the statistical error. The open symbols refer to the direct lattice QCD data. Since these data behave almost linearly in m_π^2 , we adopt the linear chiral extrapolation in m_π^2 to obtain m_{5Q} in the physical quark mass region. Note that the ordinary non-PS mesons and baryons show similar linearity in m_π^2 [71]. The closed symbols denote the results of the chiral extrapolation. We see that all the 5Q states appear above the s-wave NK^* and the d-wave NK

thresholds. As a result of the chiral extrapolation, we obtain only massive 5Q states as $m_{5Q} = 2.17(4), 2.11(4)$ GeV from the NK^* -type and the twisted NK^* -type correlators, respectively, which is too heavy to be identified with the experimentally observed $\Theta^+(1540)$. Numerical values of m_{5Q} at each hopping parameter together with their chirally extrapolated values are summarized in Table IV. To obtain a low-lying state at $m_{5Q} \simeq 1540$ MeV, a 5Q state should appear below these thresholds at least in the light quark mass region. In this case, a significantly large chiral effect is required. Of course, this point can be in principle clarified by an explicit lattice QCD calculation with chiral fermions.

B. $J^P = 3/2^+$ 5Q spectrum in PBC

We consider 5Q spectrum in $J^P = 3/2^+$ channel. $J^P = 3/2^+$ is an interesting quantum number from the view point of the diquark picture of Jaffe and Wilczek[22]. In this picture, the pair of diquarks has angular momentum one, which is combined with the spin $1/2$ of \bar{s} quark. Hence, there are two possibilities as $J^P = 1/2^+$ and $3/2^+$, i.e., the diquark picture can support $J^P = 3/2^+$ possibility as well. Its mass splits from the $J^P = 1/2^+$ state depending on a particular form of the LS-interaction. If it is massive, it is expected to have a large decay width. If it is light enough, its exotic structure may work to implement the narrow decay width as in $J^P = 1/2^+$ case.

In Fig. 3, we show the 5Q effective mass plots in PBC employing three types of interpolating fields, i.e., (a) the NK^* -type, (b) the twisted NK^* -type, (c) the diquark-type. The dotted lines indicate the s-wave N^*K^* , the p-wave NK^* and the p-wave NK thresholds in the spatial lattice of the size $L \simeq 2.15$ fm, respectively.

Fig. 3 (a) shows the 5Q effective mass plot employing the NK^* -type interpolating field. In the region, $0 \leq \tau \lesssim 17$, the contaminations of higher spectral contributions become gradually reduced. There is a flat region $18 \lesssim \tau \leq 30$, which is still afflicted with slightly large statistical errors. The single-exponential fit in this region gives $m_{5Q} = 3.34(3)$ GeV. Note that this value agrees with the s-wave N^*K^* threshold $E_{th} \simeq 3.27$ GeV. (See Table III for m_{N^*} .)

Fig. 3 (b) shows the 5Q effective mass plot corresponding to the twisted NK^* -type interpolating field. We have a rather stable plateau in the interval $21 \leq \tau \leq 27$, where the single-exponential fit is performed. We obtain $m_{5Q} = 3.11(4)$ GeV. The result is denoted by the solid line.

Fig. 3 (c) shows the 5Q effective mass plot for the diquark-type interpolating field. We find a plateau in the interval $19 \leq \tau \leq 29$, where the single-exponential fit is performed. We obtain $m_{5Q} = 3.16(2)$ GeV, which is denoted by the solid line.

Now, we perform the chiral extrapolation. In Fig. 4, m_{5Q} is plotted against m_π^2 . Circles, boxes and trian-

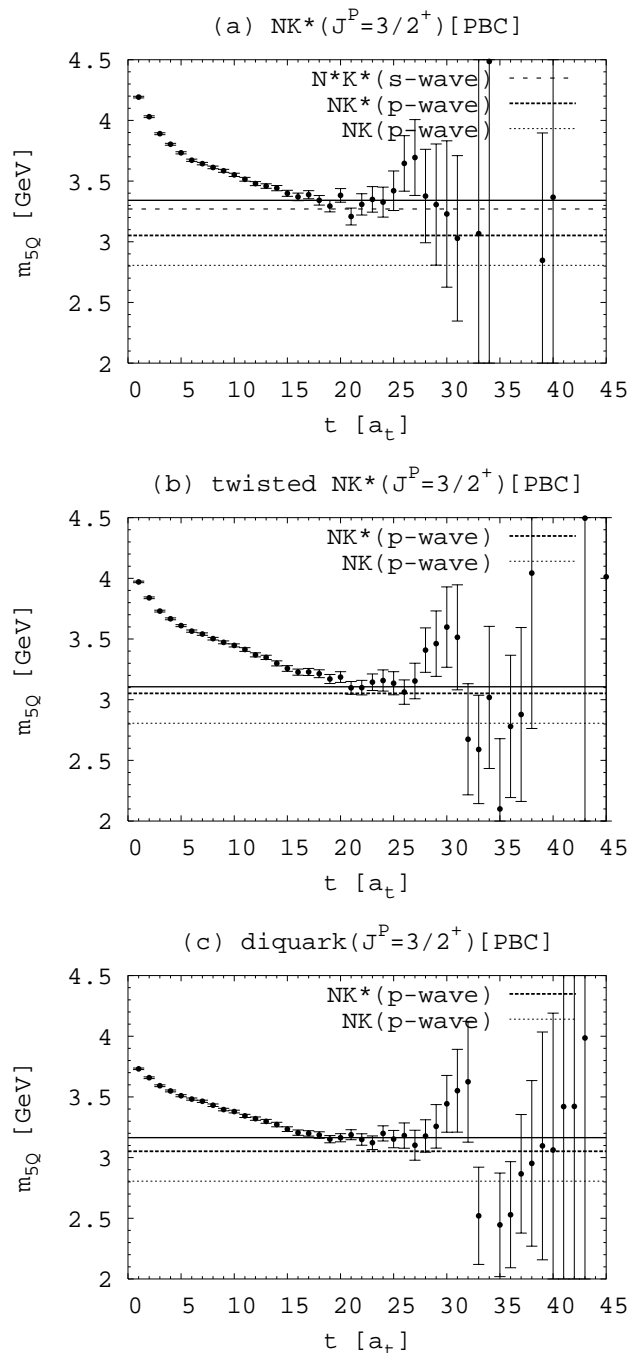


FIG. 3: The 5Q effective mass plots in $J^P = 3/2^+$ channel in PBC for three types of interpolating fields, i.e., (a) the NK^* -type, (b) the twisted NK^* -type, and (c) the diquark-type. Eq. (31) is adopted as a typical set of hopping parameters. The dotted lines indicate the s-wave N^*K^* , the p-wave NK^* and the p-wave NK thresholds in the spatial lattice size $L \simeq 2.15$ fm. The solid lines denote the results of the single-exponential fit performed in each plateau region.

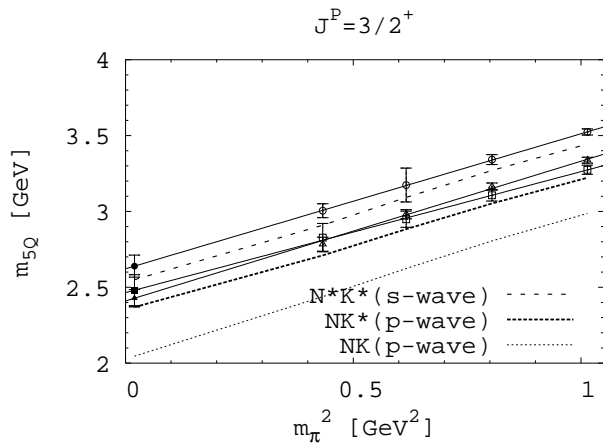


FIG. 4: m_{5Q} in $J^P = 3/2^+$ channel against m_{π}^2 for the three interpolating fields, i.e., (circle) the NK^* -type, (box) the twisted NK^* -type, and (triangle) a diquark-type [Eq. (3)]. Open symbols denote the direct lattice QCD data, while the closed symbols and the solid lines represent the results of the chiral extrapolations to the physical quark mass region.

gles denote the data obtained from the NK^* -type, the twisted NK^* -type and the diquark-type 5Q correlators, respectively. Note that the latter two agree with each other within the statistical errors.

As a result of the chiral extrapolation, we obtain $m_{5Q} = 2.64(7)$ GeV from the NK^* -type correlator, $m_{5Q} = 2.48(10)$ GeV from the twisted NK^* -type correlator, and $m_{5Q} = 2.42(6)$ GeV from the diquark-type correlator. Numerical values of m_{5Q} in $J^P = 3/2^+$ channel at each hopping parameter together with their chirally extrapolated values are also summarized in Table IV. The two data from the twisted NK^* -type and the diquark-type correlators are considered to be almost consistent with the p-wave NK^* threshold, while the data from the NK^* -type correlator seems to correspond to a more massive state, which is likely to be consistent with the $N^*K^*(s\text{-wave})$ threshold. We see again that all of our data of m_{5Q} appear above the NK^* threshold(p-wave), which is located above the artificially raised NK threshold(p-wave) due to the finiteness of the spatial lattice as $L \simeq 2.15$ fm. As a result, we are left only with such massive 5Q states.

Now, several comments are in order. (1) Ref.[67] reported the existence of a low-lying 5Q state in $J^P = 3/2^+$ channel using NK^* -type interpolating field. However, we have not observed such a low-lying 5Q state in our calculation. (2) Recall that, except for a single calculation[59], lattice QCD calculations indicate that $J^P = 1/2^+$ state is heavy [57, 58, 60, 61, 62, 63, 64, 65, 66], for instance $m_{5Q} \simeq 2.25$ GeV in Ref.[61]. From the viewpoint of the diquark picture, it could be natural to obtain such massive 5Q states in $J^P = 3/2^+$ channel. If there were a low-lying 5Q state in $J^P = 3/2^+$ channel, then the diquark picture could suggest also a low-lying 5Q state in

$J^P = 1/2^+$ channel nearby.

V. ANALYSIS WITH HBC

In the previous section, we have only massive 5Q states, which are obtained by using the linear chiral extrapolation in m_{π}^2 . However, the chiral behavior may deviate from a simple linear one in the light quark mass region, which could lead to somewhat less massive states. Considering this, we think it of worth at this stage to analyze whether our 5Q states are compact 5Q resonances or not. This is done by switching the spatial periodic BC to the hybrid BC(HBC) introduced in Sect. II.

A. $J^P = 3/2^-$ 5Q spectrum in HBC

Fig. 5 shows the 5Q effective mass plots in HBC employing the three types of interpolating fields, i.e., (a) the NK^* -type, (b) the twisted NK^* -type, and (c) the diquark type. These figures should be compared with their PBC counterparts in Fig. 1. The dotted lines denote the s-wave NK^* and the d-wave NK thresholds. For the typical set of hopping parameters, i.e., Eq. (31), the s-wave NK^* threshold(the thick dotted line) is raised up by ~ 180 MeV, and the d-wave NK threshold(the thin dotted line) is lowered down by ~ 70 MeV due to HBC in the finite spatial extent as $L \simeq 2.15$ fm. (See Table I.)

Fig. 5 (a) shows the 5Q effective mass plot for the NK^* -type interpolating field in HBC. We find a plateau in the interval $23 \leq \tau \leq 35$, where the single-exponential fit is performed leading to $m_{5Q} = 2.98(1)$ GeV, which is denoted by the solid line. We see that m_{5Q} is raised up by 80 MeV due to HBC. The value of m_{5Q} is consistent with the s-wave NK^* threshold within the statistical error. Therefore, we regard this state as an NK^* scattering state.

Fig. 5 (b) shows the 5Q effective mass plot for the twisted NK^* -type interpolating field. We find a plateau in the interval $24 \leq \tau \leq 35$, where the single exponential fit is performed leading to $m_{5Q} = 2.98(1)$ GeV, which is denoted by the solid line. The situation is similar to the NK^* -interpolating field case. We see that m_{5Q} is raised up by 90 MeV due to HBC. Since the value is consistent with the s-wave NK^* threshold within the statistical error, we regard it as an NK^* scattering state.

Fig. 5 (c) shows the 5Q effective mass plot for the diquark-type interpolating field. We see that it is afflicted with considerable size of statistical errors as before, due to which the best-fit is not performed.

In this way, all of our 5Q states in $J^P = 3/2^-$ channel turn out to be NK^* scattering states. More precisely, we do not observe any compact 5Q resonance states in $J^P = 3/2^-$ channel below the raised s-wave NK^* threshold, i.e., in the following region:

$$E \lesssim \sqrt{m_N^2 + \vec{p}_{\min}^2} + \sqrt{m_{K^*}^2 + \vec{p}_{\min}^2}, \quad (34)$$

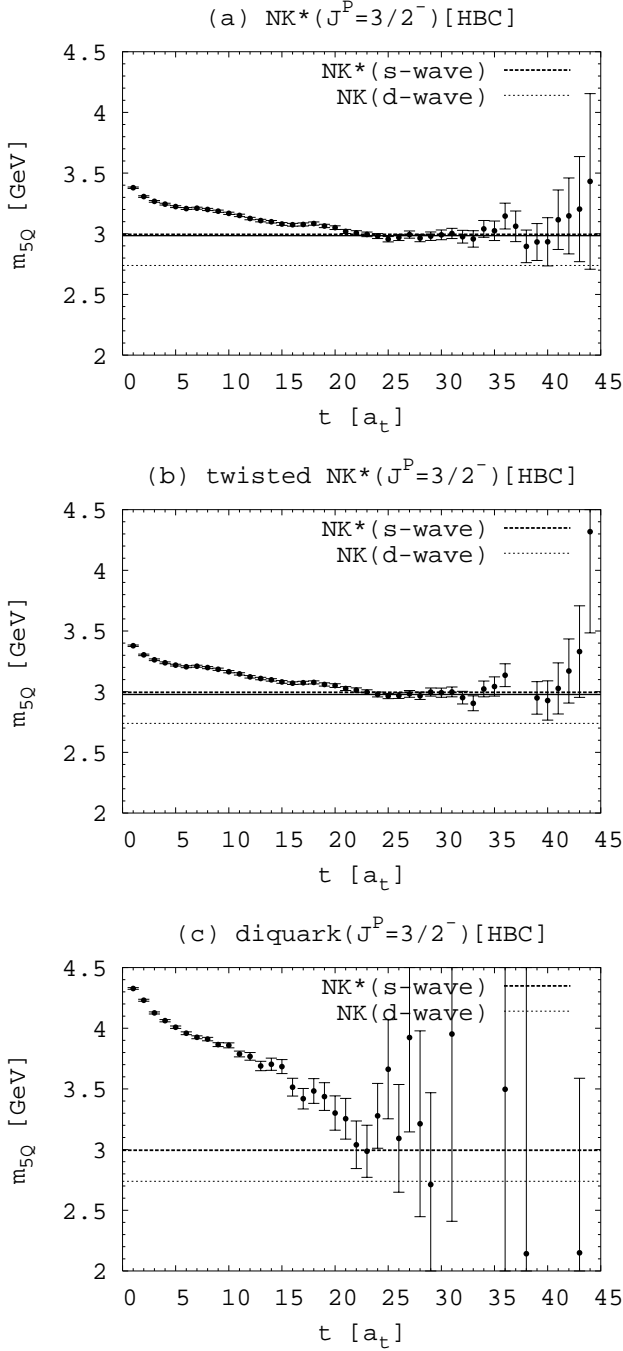


FIG. 5: The 5Q effective mass plots in $J^P = 3/2^-$ channel in HBC for three types of interpolating fields, i.e., (a) the NK^* -type, (b) the twisted NK^* -type, and (c) the diquark-type. The meanings of the dotted lines and the solid lines are the same as in Fig. 1.

with $|\vec{p}_{\min}| \simeq 499$ MeV.

B. $J^P = 3/2^+$ 5Q spectrum in HBC

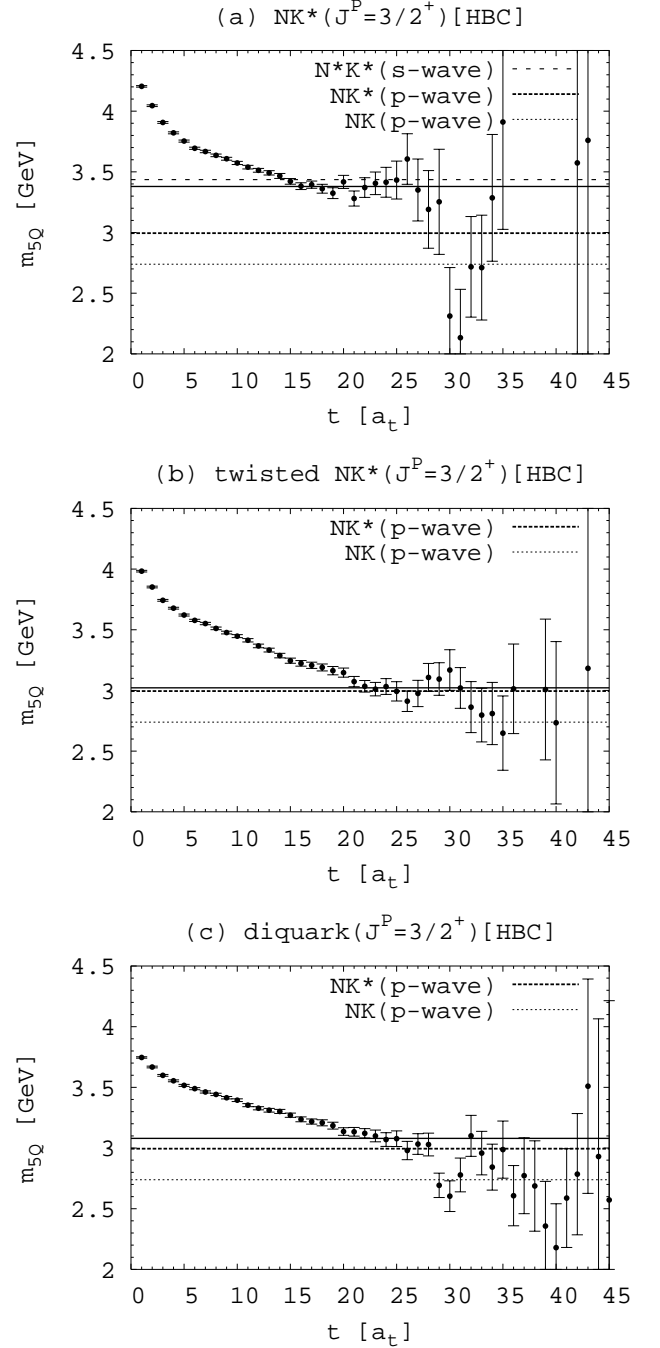


FIG. 6: 5Q effective mass plots in $J^P = 3/2^+$ channel in HBC for three types of interpolating fields (a) the NK^* -type, (b) the twisted NK^* -type, and (c) the diquark-type. The meanings of the dotted and the solid lines are the same as in Fig. 3.

Fig. 6 shows the 5Q effective mass plots in HBC em-

ploying the three types of interpolating fields, i.e., (a) the NK^* -type, (b) the twisted NK^* -type, and (c) the diquark-type. These figures should be compared with their PBC counterparts in Fig. 3. The meanings of the dotted and the solid lines are the same as in Fig. 3.

HBC may not be useful in $J^P = 3/2^+$ channel, since it induces only minor changes in the two-particle spectra. For the typical set of hopping parameters, i.e., Eq. (31), the p-wave NK^* threshold is lowered down only by ~ 60 MeV, and the p-wave NK threshold is lowered down only by ~ 70 MeV. We see that these shifts are rather small. This is because they are induced by the changes in the minimum non-vanishing momentum, i.e., $|\vec{p}_{\min}| = 2\pi/L \simeq 576$ MeV to $\sqrt{3}\pi/L \simeq 499$ MeV as mentioned before. In $J^P = 3/2^+$ channel, N^*K^* (s-wave) threshold shows the most drastic change, i.e., the upper shift by 170 MeV, which however plays a less significant role, since its location is at rather high energy.

Fig. 6 (a) shows the 5Q effective mass plot employing the NK^* -type interpolating field. There is a flat region $16 \leq \tau \lesssim 25$, which is still afflicted with slightly large statistical errors. The single-exponential fit in this region leads to $m_{5Q} = 3.38(2)$ GeV, which is denoted by the solid line. We see that m_{5Q} is raised up by 40 MeV. Although the shift of 40 MeV is rather small, m_{5Q} is again almost consistent with the s-wave N^*K^* threshold. Considering its rather large statistical error, this 5Q state is likely to be an s-wave N^*K^* scattering state. To draw a more solid conclusion on this state, it is necessary to improve the statistics further more.

Fig. 6 (b) shows the 5Q effective mass plot employing the twisted NK^* -type interpolating field. There is a plateau in the interval $23 \leq \tau \leq 31$, where we perform the single-exponential fit. The result $m_{5Q} = 3.02(3)$ GeV is denoted by the solid line. We see that m_{5Q} is lowered down by 90 MeV, which is considered to be consistent with the shift of the NK^* (p-wave) threshold. Therefore, this state is likely to be an NK^* (p-wave) scattering state.

Fig. 6 (c) shows the 5Q effective mass plot employing the diquark-type interpolating field. Although the data is slightly noisy, there is a plateau in the interval $23 \leq \tau \leq 28$. A single-exponential fit in this plateau region leads to $m_{5Q} = 3.08(4)$ GeV, which is denoted by the solid line. m_{5Q} is lowered down by 80 MeV due to HBC. The situation is similar to Fig. 6 (b). This state is likely to be an NK^* (p-wave) scattering state.

In this way, all of our 5Q states are likely to be either N^*K^* (s-wave) or NK^* (p-wave) states rather than compact 5Q resonance states. Of course, because HBC induces only minor changes in the 5Q spectrum in $J^P = 3/2^+$ channel, and also because 5Q correlators still involve considerable size of statistical error, more statistics is desirable to draw a more solid conclusion on the real nature of these 5Q states. Here, we can at least state that these 5Q states are all massive, which locate above NK^* (p-wave) threshold.

VI. SUMMARY AND CONCLUSION

We have studied $J^P = 3/2^\pm$ penta-quark(5Q) baryons in anisotropic lattice QCD at the quenched level with a large number of gauge field configurations as $N_{\text{conf}} = 1000$ for high precision measurements. We emphasize that the spin of $\Theta^+(1540)$ has not yet determined experimentally, and that the $J^P = 3/2^-$ assignment provides us with one of the possible solutions to the puzzle of the narrow decay width of $\Theta^+(1540)$ [43]. We have employed the standard Wilson gauge action on the anisotropic lattice of the size $12^3 \times 96$ with the renormalized anisotropy $a_s/a_t = 4$ at $\beta = 5.75$, which leads to $a_s \simeq 0.18$ fm and $a_t \simeq 0.045$ fm. We have found that correlators of 5Q baryons in $J^P = 3/2^\pm$ channels are rather noisy. Hence, the large statistics as $N_{\text{conf}} = 1000$ has played a key role to get a solid result in our calculation. For the quark part, we have employed $O(a)$ -improved Wilson (clover) action with four values of the hopping parameters as $\kappa = 0.1210(0.0010)0.1240$, which roughly cover the quark mass region as $m_s \lesssim m \lesssim 2m_s$. To avoid the contaminations of higher spectral contributions, we have employed the spatially extended source in the 5Q correlators.

We have examined several types of the 5Q interpolating fields as (a) the NK^* -type, (b) the (color-)twisted NK^* -type, (c) the diquark-type. In $J^P = 3/2^-$ channel, there are plateaus in the effective mass plots for the NK^* -type and the twisted NK^* -type interpolating field, whereas no plateau has been identified in that for the diquark-type interpolating field due to the significantly large statistical error. The former two give almost identical results. We have employed the linear chiral extrapolations in m_π^2 , which have lead to $m_{5Q} \simeq 2.17$ and 2.11 GeV for the NK^* -type and the twisted NK^* -type 5Q correlators, respectively. In $J^P = 3/2^+$ channel, we have recognized plateaus in all the three effective mass plots. However, the plateau for the NK^* -type interpolating field is located at a somewhat higher energy than the other two. The chiral extrapolations have lead to $m_{5Q} \simeq 2.64$ GeV for the NK^* -type correlator, $m_{5Q} \simeq 2.48$ GeV for the twisted NK^* -type correlator, and $m_{5Q} \simeq 2.42$ GeV for the diquark-type correlator. In this way, our data have not supported low-lying 5Q states in both $J^P = 3/2^\pm$ channels. All the 5Q states have been observed to appear above the d/p-wave NK threshold, which is artificially raised up by a few hundred MeV due to the finiteness of the spatial lattice as $L \simeq 2.15$ fm. Note that, to obtain low-lying 5Q states in $J^P = 3/2^\pm$ channel, a 5Q state should appear below the raised NK threshold(p/d-wave) at least in the light quark mass region.

In order to clarify whether the observed states are compact 5Q resonances or not, we have performed an analysis with hybrid boundary condition(HBC), which was recently proposed by Ref.[61]. In $J^P = 3/2^-$ channel, our 5Q states observed in the NK^* -type and the twisted NK^* -type correlators have turned out to be s-wave NK^* scattering states. In $J^P = 3/2^+$ channel, for the twisted

NK*-type and the diquark-type correlators, the observed 5Q states are most likely to be NK*(p-wave) scattering states. For the other one, i.e., the NK*-type interpolating field, although more statistics is needed to draw a definite conclusion, it is most likely to be an s-wave N*K* scattering state. Note that, since HBC does not affect the two-particle spectra so much in $J^P = 3/2^+$ channel, it is not easy to elucidate the natures of the 5Q states only with HBC. At any rate, whatever the real nature of these 5Q states may be, they result in a considerably massive state in the physical quark mass region, which cannot be identified as $\Theta^+(1540)$ without involving a significantly large chiral contribution.

In this way, we have not obtained any relevant signals for low-lying compact 5Q resonance states in $J^P = 3/2^\pm$ channel below 2.1 GeV in this paper, although the $J^P = 3/2^-$ possibility provides us with one of the possible solutions to the puzzle of the narrow decay width of $\Theta^+(1540)$. To get more solid conclusion on the pentaquark, it is important to perform the systematic studies of the 5Q states with the various quantum numbers in lattice QCD with more sophisticated conditions. For instance, it is desired to use (1) unquenched full lattice QCD, (2) finer and larger volume lattice, (3) chiral fermion with small mass, (4) more sophisticated interpolating field corresponding to the diquark picture and so on. In any case, the mysterious exotic hadron of the pentaquark would be much clarified in future studies of lattice QCD as well as in the future experiments.

Acknowledgments

We thank A. Hosaka, J. Sugiyama, T. Shinozaki for useful information and discussions. M. O and H. S are supported in part by Grant for Scientific Research ((B) No. 15340072 and (C) No. 16540236) from the Ministry of Education, Culture, Sports, Science and Technology, Japan. T. D. is supported by Special Postdoctoral Research Program of RIKEN. Y. N. is supported by 21st Century COE Program of Nagoya University. The lattice QCD Monte Carlo calculations have been performed on NEC-SX5 at Osaka University.

APPENDIX A: SPECTRAL REPRESENTATION

Considering the importance of the parity determination of Θ^+ , we present a brief derivation of the spectral representation of Rarita-Schwinger correlators, i.e., Eq. (8), with Eq. (11). In this section, gamma matrices are represented in Minkowskian form (See Ref.[79]). To avoid unnecessary complexities, we derive only $J^P = 3/2^\pm$ parts. The $J^P = 1/2^\pm$ parts can be obtained as a slight modification, on which we will make a comment at the end of the section.

We first consider the coupling of our interpolating fields ψ_μ to $J^P = 3/2^\pm$ (anti-)baryon states. Due to Eq. (6), our interpolating fields, i.e., Eqs. (1),(2) and (3) have the negative intrinsic parity. Hence, their couplings

to $J^P = 3/2^-$ (anti-)baryons are parameterized in the following way:

$$\begin{aligned} \langle 0|\psi_\mu(0)|B_{3/2^-}(k, \alpha)\rangle &= \lambda_{3/2^-} u_\mu(m_{3/2^-}; k, \alpha) \quad (\text{A1}) \\ \langle 0|\bar{\psi}_\mu(0)|\bar{B}_{3/2^-}(k, \alpha)\rangle &= \lambda_{3/2^-}^* \bar{v}_\mu(m_{3/2^-}; k, \alpha), \end{aligned}$$

where $|B_{3/2^-}(k, \alpha)\rangle$ and $|\bar{B}_{3/2^-}(k, \alpha)\rangle$ denote $J^P = 3/2^-$ (anti-)baryon states with momentum k , helicity α , and mass $m_{3/2^-}$. $u_\mu(m; k, \alpha)$ and $v_\mu(m; k, \alpha)$ denote the Rarita-Schwinger spinors for $J = 3/2$ particles with momentum k , helicity α and mass m [73, 74, 75]. Eqs. (1),(2) and (3) couples to $J^P = 3/2^+$ (anti-)baryons as well. In this case, their couplings involve γ_5 in the following way:

$$\begin{aligned} \langle 0|\psi_\mu(0)|B_{3/2^+}(k, \alpha)\rangle &= \lambda_{3/2^+} \gamma_5 u_\mu(m_{3/2^+}; k, \alpha) \quad (\text{A2}) \\ \langle 0|\bar{\psi}_\mu(0)|\bar{B}_{3/2^+}(k, \alpha)\rangle &= -\lambda_{3/2^+}^* \bar{v}_\mu(m_{3/2^+}; k, \alpha) \gamma_5, \end{aligned}$$

where $|B_{3/2^+}(k, \alpha)\rangle$ and $|\bar{B}_{3/2^+}(k, \alpha)\rangle$ denote $J^P = 3/2^+$ (anti-)baryon states with momentum k , helicity α and mass $m_{3/2^+}$. “-” originates from the anti-commutativity of γ_0 and γ_5 .

To derive the spectral representation, the best way would be to express it in the operator representation in the following way:

$$G_{\mu\nu}(\tau, \vec{x}) = Z^{-1} \text{Tr} \left(e^{-\beta H} T_\tau [\psi_{\mu'}(\tau, \vec{x}) \bar{\psi}_\mu(0)] \right), \quad (\text{A3})$$

where β denotes the temporal extent of the lattice, $H \equiv H_{\text{QCD}}$ denotes the QCD Hamiltonian, $Z \equiv \text{Tr}(e^{-\beta H})$ denotes the partition function, and $T_\tau[*]$ represents the time-ordered product along the imaginary time direction. The interpolating fields are represented in the Heisenberg picture in imaginary-time, i.e., $\psi_\mu(\tau, \vec{x}) = e^{\tau H} \psi_\mu(0, \vec{x}) e^{-\tau H}$ and $\bar{\psi}_\mu(\tau, \vec{x}) = e^{\tau H} \bar{\psi}_\mu(0, \vec{x}) e^{-\tau H}$. By restricting ourselves to the interval $0 \leq \tau < \beta$, Eq. (A3) reduces to

$$G_{\mu\nu}(\tau, \vec{x}) = \text{Tr} \left(\frac{e^{-\beta H}}{Z} \psi_{\mu'}(\tau, \vec{x}) \bar{\psi}_\mu(0) \right). \quad (\text{A4})$$

Note that it can be equivalently expressed as

$$G_{\mu\nu}(\tau, \vec{x}) = \text{Tr} \left(\psi_{\mu'}(\tau - \beta, \vec{x}) \frac{e^{-\beta H}}{Z} \bar{\psi}_\mu(0) \right). \quad (\text{A5})$$

In the large β limit, we have $e^{-\beta H}/Z \simeq |0\rangle\langle 0|$, which is inserted into Eq. (A4) and Eq. (A5). Note that the resulting two expressions serve as independent contributions to the original “Tr”, i.e., Eq. (A4) (or Eq. (A5)). Hence, we keep these two contributions to obtain

$$\begin{aligned} G_{\mu\nu}(\tau, \vec{x}) & \quad (\text{A6}) \\ & \simeq \langle 0|\psi_{\mu'}(\tau, \vec{x}) \bar{\psi}_\mu(0)|0\rangle + \langle 0|\bar{\psi}_\mu(0) \psi_{\mu'}(\tau - \beta, \vec{x})|0\rangle. \end{aligned}$$

Note that the 1st term corresponds to the forward propagation, whereas the 2nd term to the backward propagation. By inserting single-(anti-)baryon intermediate states, and by using Eq. (A1) and Eq. (A2), we are left with

$$\begin{aligned}
G_{\mu\nu}(\tau, \vec{x}) &= \sum_{\alpha=1}^4 \int \frac{d^3k}{(2\pi)^3} \frac{m_{3/2^+}}{k_0} e^{-\tau k_0} \langle 0 | \psi_{\mu'}(\vec{x}) | B_{3/2^+}(k, \alpha) \rangle \langle B_{3/2^+}(k, \alpha) | \bar{\psi}_{\mu}(0) | 0 \rangle + \dots \\
&= |\lambda_{3/2^-}|^2 \int \frac{d^3k}{(2\pi)^3} \frac{m_{3/2^-}}{k_0} (-1) P_{\mu\nu}^{(3/2)}(k) \left[e^{-\tau k_0} e^{i\vec{k}\cdot\vec{x}} \left(\frac{m_{3/2^-} + \not{k}}{2m_{3/2^-}} \right) + e^{-(\beta-\tau)k_0} e^{-i\vec{k}\cdot\vec{x}} \left(\frac{m_{3/2^-} - \not{k}}{2m_{3/2^-}} \right) \right] \\
&\quad - |\lambda_{3/2^+}|^2 \int \frac{d^3k}{(2\pi)^3} \frac{m_{3/2^+}}{k_0} (-1) P_{\mu\nu}^{(3/2)}(k) \left[e^{-\tau k_0} e^{i\vec{k}\cdot\vec{x}} \left(\frac{m_{3/2^+} - \not{k}}{2m_{3/2^+}} \right) + e^{-(\beta-\tau)k_0} e^{-i\vec{k}\cdot\vec{x}} \left(\frac{m_{3/2^+} + \not{k}}{2m_{3/2^+}} \right) \right],
\end{aligned} \tag{A7}$$

where $k_0 \equiv \sqrt{m_{3/2^-}^2 + \vec{k}^2}$ for $J^P = 3/2^-$, $k_0 \equiv \sqrt{m_{3/2^+}^2 + \vec{k}^2}$ for $J^P = 3/2^+$, and the following identities are used.

$$\begin{aligned}
\sum_{\alpha=1}^4 u_{\mu}(m; k, \alpha) \bar{u}_{\nu}(m; k, \alpha) &= -\frac{m + \not{k}}{2m} P_{\mu\nu}^{(3/2)}(k) \\
\sum_{\alpha=1}^4 v_{\mu}(m; k, \alpha) \bar{v}_{\nu}(m; k, \alpha) &= \frac{m - \not{k}}{2m} P_{\mu\nu}^{(3/2)}(k),
\end{aligned} \tag{A8}$$

where $P_{\mu\nu}^{(3/2)}(k)$ is the spin 3/2 projection operator defined as

$$P_{\mu\nu}^{(3/2)}(k) \equiv g_{\mu\nu} - \frac{1}{3}\gamma_{\mu}\gamma_{\nu} - \frac{1}{3k^2}(\not{k}\gamma_{\mu}k_{\nu} + k_{\mu}\gamma_{\nu}\not{k}). \tag{A9}$$

By performing the integration over \vec{x} for zero-momentum projection, and by replacing the Minkowskian gamma matrices by their Euclidean counterparts, we finally arrive at the spectral representation (Eq. (8) with Eq. (11)).

The derivation of the spin 1/2 parts is obtained by repeating a similar procedure using the following param-

eterizations instead of Eq. (A1) and Eq. (A2) as

$$\begin{aligned}
\langle 0 | \psi_{\mu}(0) | B_{1/2^-}(k, \alpha) \rangle & \\
&= \left(\lambda_{1/2^-} \gamma_{\mu} + \lambda'_{1/2^-} k_{\mu} \right) u(m_{1/2^-}; k, \alpha) \\
\langle 0 | \bar{\psi}_{\mu}(0) | \bar{B}_{1/2^-}(k, \alpha) \rangle & \\
&= \bar{v}(m_{1/2^-}; k, \alpha) \left(\lambda_{1/2^-}^* \gamma_{\mu} - \lambda'_{1/2^-} k_{\mu} \right) \\
\langle 0 | \psi_{\mu}(0) | B_{1/2^+}(k, \alpha) \rangle & \\
&= \left(\lambda_{1/2^+} \gamma_{\mu} + \lambda'_{1/2^+} k_{\mu} \right) \gamma_5 u(m_{1/2^+}; k, \alpha) \\
\langle 0 | \bar{\psi}_{\mu}(0) | \bar{B}_{1/2^+}(k, \alpha) \rangle & \\
&= -\bar{v}(m_{1/2^+}; k, \alpha) \gamma_5 \left(\lambda_{1/2^+}^* \gamma_{\mu} - \lambda'_{1/2^+} k_{\mu} \right),
\end{aligned} \tag{A10}$$

where $|B_{1/2^{\pm}}(k, \alpha)\rangle$ and $|\bar{B}_{1/2^{\pm}}(k, \alpha)\rangle$ denote the $J^P = 1/2^{\pm}$ (anti-)baryon states with momentum k , helicity α and mass $m_{1/2^{\pm}}$. $u(m; k, \alpha)$ and $v(m; k, \alpha)$ denote the Dirac bispinors for spin 1/2 particles with mass m , momentum k and helicity α . $\lambda_{1/2^{\pm}}$ and $\lambda'_{1/2^{\pm}}$ represent the couplings to $J^P = 1/2^{\pm}$ (anti-)baryons.

-
- [1] LEPS Collaboration, T. Nakano *et al.*, Phys. Rev. Lett. **91**, 012002 (2003).
[2] NA49 Collaboration (C. Alt *et al.*), Phys. Rev. Lett. **92**, 042003 (2004).
[3] H1 Collaboration (A. Aktas *et al.*), Phys. Lett. **B588**, 17 (2004).
[4] Belle Collaboration, S.K. Choi *et al.*, Phys. Rev. Lett. **91**, 262001 (2003); CDF II Collaboration, D. Acosta *et al.*, Phys. Rev. Lett. **93**, 072001 (2004); P. Pakhlov (For the Belle Collaboration), hep-ex/0412041; Belle Collaboration, S.-K. Choi *et al.*, Phys. Rev. Lett. **94**, 182002 (2005); T. Suzuki *et al.*, Phys. Lett. **B597**, 263 (2004). BABAR Collaboration, B. Aubert *et al.*, Phys. Rev. Lett. **90**, 242001 (2003); BELLE Collaboration, S.-K. Choi *et al.*, Phys. Rev. Lett. **91**, 262002 (2003); CLEO Collaboration, D. Besson *et al.*, Phys. Rev. **D68**, 032002 (2003).
[5] D. Diakonov, V. Petrov and M.V. Polyakov, Z. Phys. **A359**, 305 (1997).
[6] R.L. Jaffe, SLAC-PUB-1774 (1976).
[7] D. Strottman, Phys. Rev. **D20**, 748 (1979).
[8] H. Weigel, Eur. Phys. J. **A2**, 391, (1998).
[9] M. Praszalowicz, Phys. Lett. **B575**, 234 (2003); M. Praszalowicz, in : M. Jezabek, M. Praszalowicz (Eds.), Proceedings of the Workshop on Skyrmions and Anomalies, World Scientific, Singapore, 1987, p. 112.
[10] DIANA Collaboration, V.V. Barmin *et al.*, Phys. Atom. Nucl. **66**, 1715 (2003).
[11] CLAS Collaboration, S. Stepanyan *et al.*, Phys. Rev. Lett. **91**, 252001 (2003).
[12] SAPHIR Collaboration, J. Barth *et al.*, Phys. Lett. **B572**, 127 (2003).
[13] A.E. Asratyan, A.G. Dolgolenko, M.A. Kubantsev, Phys. Atom. Nucl. **67**, 682 (2004); CLAS Collaboration, V. Kubarovsky, *et al.*, Phys. Rev. Lett. **92**, 032001 (2004); HERMES Collaboration, A. Airapetian, *et al.*, Phys. Lett. **B585**, 213 (2004); SVD Collaboration, A. Aleev, *et al.*, hep-ex/0401024; COSY-TOF Collaboration, M. Abdel-Bary, *et al.*, Phys. Lett. **B595**, 127 (2004); ZEUS Collaboration, S. Chekanov, *et al.*, Phys. Lett. **B591**, 7 (2004);
[14] BES Collaboration, J.Z. Bai *et al.*, Phys. Rev. **D70**, 012004 (2004); HERA-B Collaboration, K.T. Knoepfle

- et al.*, J. Phys. **G30**, S1363 (2004); PHENIX Collaboration, C. Pinkenburg *et al.*, J. Phys. **G30**, S1201 (2004); HERA-B Collaboration, I. Abt *et al.*, Phys. Rev. Lett **93**, 212003 (2004); SPHINX Collaboration, Y.-M. Antipov *et al.*, Eur. Phys. J. **A21**, 455 (2004); CDF Collaboration, I.V. Gorelov *et al.*, hep-ex/0408025; HyperCP Collaboration, M.J. Longo *et al.*, Phys. Rev. **D70**, 111101 (2004); BABAR Collaboration, B. Aubert *et al.*, hep-ex/0408064; S.R. Armstrong, Nucl. Phys. B(Proc. Suppl.)**142**, 364 (2005); BELLE Collaboration, K. Abe *et al.*, hep-ex/0409010; ALEPH Collaboration, S. Schael *et al.*, Phys. Lett. **B599**, 1 (2004); CDF Collaboration, D.O. Litvintsev *et al.*, Nucl. Phys. B(Proc. Suppl.)**142**, 374 (2005); FOCUS Collaboration, K. Stenson *et al.*, hep-ex/0412021; BELLE Collaboration, R. Mizuk *et al.*, hep-ex/0411005;
- [15] For recent review of the experimental status, K.H. Hicks, hep-ex/0504027, and references therein.
- [16] M. Oka, Prog. Theor. Phys. **112**, 1 (2004), and references therein.
- [17] S.L. Zhu, Int. J. Mod. Phys. **A19**, 3439 (2004), and references therein.
- [18] T.D. Cohen, Phys. Lett. **B581**, 175 (2004).
- [19] N. Itzhaki, I.R. Klebanov, P. Ouyang, L. Rastelli, Nucl. Phys. **B684**, 264 (2004).
- [20] H.-Ch. Kim, Phys. Lett. **B585**, 99 (2004).
- [21] A. Hosaka, Phys. Lett. **B571**, 55 (2003).
- [22] R.L. Jaffe and F. Wilczek, Phys. Rev. Lett. **91**, 232003 (2003).
- [23] M. Karliner and H.J. Lipkin, Phys. Lett. **B575**, 249 (2003).
- [24] C.E. Carlson, C.D. Carone, H.J. Kwee, V. Nazaryan, Phys. Lett. **B579**, 52 (2004).
- [25] Fl. Stancu and D.O. Riska, Phys. Lett. **B575**, 242 (2003).
- [26] B.K. Jennings and K. Maltman, Phys. Rev. **D69**, 094020 (2004).
- [27] L.Y. Glozman, Phys. Lett. **B575**, 18 (2003).
- [28] Y. Kanada-En'yo, O. Morimatsu, and T. Nishikawa, Phys. Rev. **C71**, 0452002 (2005).
- [29] P. Bicudo, and G.M. Marques, Phys. Rev. **D69**, 011503 (2004).
- [30] F.J. Llanes-Estrada, E. Oset, and V. Mateu, Phys. Rev. **C69**, 055203 (2004).
- [31] C.E. Carlson, C.D. Carone, H.J. Kwee and V. Nazaryan, Phys. Lett. **B573**, 101 (2003).
- [32] F. Huang, Z.Y. Zhang, Y.W. Yu, and B.S. Zou, Phys. Lett. **B586**, 69 (2004).
- [33] T. Shinozaki, M. Oka, and S. Takeuchi, Phys. Rev. **D71**, 074025 (2005).
- [34] S.-L. Zhu, Phys. Rev. Lett. **91**, 232002 (2003).
- [35] R.D. Matheus, F.S. Navarra, M. Nielsen, R. Rodrigues da Silva, and S.H. Lee, Phys. Lett. **B578**, 323 (2004).
- [36] J. Sugiyama, T. Doi, and M. Oka, Phys. Lett. **B 581**, 167 (2004).
- [37] Y. Oh, H. Kim, and S.H. Lee, Phys. Rev. **D69**, 094009 (2004).
- [38] Y. Maezawa, T. Maruyama, N. Itagaki, and T. Hatsuda, Acta Phys. Hung. **A22**, 61 (2005).
- [39] I.M. Narodetskii, Yu.A. Simonov, M.A. Trusov, and A.I. Veselov, Phys. Lett. **B578**, 318 (2004).
- [40] M. Bando, T. Kugo, A. Sugamoto, and S. Terunuma, Prog. Theor. Phys. **112**, 325 (2004).
- [41] H. Suganuma, T.T. Takahashi, F. Okiharu, and H. Ichie, Talk given at International Workshop *PEN-TAQUARK04*, July 2004, SPring-8, Harima, Japan.
- [42] F. Okiharu, H. Suganuma, and T.T. Takahashi, Phys. Rev. Lett. **94**, 192001 (2005), hep-lat/0407001; hep-lat/0412012; H. Suganuma, T.T. Takahashi, F. Okiharu, and H. Ichie, Proc. of QCD Down Under, Adelaide, March 2004, Nucl. Phys. **B(Proc. Suppl.)141**, 92 (2005).
- [43] A. Hosaka, M. Oka, and T. Shinozaki, hep-ph/0409102.
- [44] T. Nishikawa, Y. Kanada-En'yo, and O. Morimatsu, Phys. Rev. **D71**, 076004 (2005).
- [45] S. Takeuchi, and K. Shimizu, hep-ph/0410286.
- [46] J. Sugiyama, T. Doi, and M. Oka, spin 3/2 penta-quark in preparation.
- [47] W. Wei, P.-Z. Huang, H.-X. Chen, and S.-L. Zhu, hep-ph/0503166.
- [48] T. Inoue, V.E. Lyubovitskij, Th. Gutsche, and A. Faessler, hep-ph/0407305.
- [49] R. Jaffe and F. Wilczek, Phys. Rev. **D69**, 114017 (2004).
- [50] F. Huang, Z.Y. Zhang, and Y.W. Yu, hep-ph/0411222.
- [51] S. Capstick, P.R. Page, and W. Roberts, Phys. Lett. **B570**, 185 (2003).
- [52] J.J. Dudek, and F.E. Close, Phys. Lett. **B583** 278 (2004).
- [53] T. Hyodo, and A. Hosaka, Phys. Rev. **D71**, 054017 (2005).
- [54] S.I. Nam, A. Hosaka, H.-C. Kim, hep-ph/0505134.
- [55] Particle Data Group, S. Eidelman *et al.*, Phys. Lett. **B592**, 1 (2004).
- [56] T. Kishimoto, and T. Sato, hep-ex/0312003.
- [57] F. Csikor, Z. Fodor, S.D. Katz, and T.G. Kovacs, JHEP **0311**, 070 (2003).
- [58] S. Sasaki, Phys. Rev. Lett. **93**, 152001 (2004).
- [59] T.W. Chiu and T.H. Hsieh, hep-ph/0403020.
- [60] N. Mathur, F.X. Lee, A. Alexandrou, C. Bennhold, Y. Chen, S.J. Dong, T. Draper, I. Horváth, K.F. Liu, S. Tamhankar, and J.B. Zang, Phys. Rev. **D70**, 074508 (2004).
- [61] N. Ishii, T. Doi, H. Iida, M. Oka, F. Okiharu, and H. Suganuma, Phys. Rev. **D71**, 034001 (2005).
- [62] T.T. Takahashi, T. Kunihiro, T. Onogi, and T. Umeda, hep-lat/0503019, Phys. Rev. **D** (2005) in press.
- [63] B.G. Lasscock, J. Hedditch, D.B. Leinweber, W. Melnitchouk, A.W. Thomas, A.G. Williams, R.D. Young, and J.M. Zanotti, hep-lat/0503008.
- [64] C. Alexandrou and A. Tsapalis, hep-lat/0503013.
- [65] F. Csikor, Z. Fodor, S.D. Katz, T.G. Kovács, and B.C. Tóth, hep-lat/0503012.
- [66] K. Holland, and K.J. Juge, hep-lat/0504007.
- [67] B.G. Lasscock, D.B. Leinweber, W. Melnitchouk, A.W. Thomas, A.G. Williams, R.D. Young, J.M. Zanotti, hep-lat/0504015.
- [68] G.T. Fleming, hep-lat/0501011
- [69] T.R. Klassen, Nucl. Phys. **B533**, 557 (1998).
- [70] H. Matsufuru, T. Onogi, and T. Umeda, Phys. Rev. **D64**, 114503 (2001).
- [71] Y. Nemoto, N. Nakajima, H. Matsufuru, and H. Suganuma, Phys. Rev. **D68**, 094505 (2003).
- [72] N. Ishii, H. Suganuma, and H. Matsufuru, Phys. Rev. **D66**, 094506 (2002); Phys. Rev. **D66**, 014507 (2002).
- [73] B.L. Ioffe, Nucl. Phys. **B188**, 317 (1981).
- [74] M. Benmerrouche, R.M. Davidson, and N.C. Mukhopadhyay, Phys. Rev. **C39**, 2339 (1989).
- [75] T.R. Hemmert, B.R. Holstein, and J. Kambor, J. Phys. **G24**, 1831 (1998).
- [76] I. Montvay and G. Münster, "Quantum Fields on a Lat-

- tice*”, (Cambridge University Press, Cambridge, England, 1994), p. 1.
- [77] R.L. Jaffe, Nucl. Phys. B(Proc. Suppl.) **142**, 343 (2004).
- [78] N. Ishii, T. Doi, Y. Nemoto, M. Oka, H. Suganuma, a talk given at Japan-US Workshop on *Electromagnetic Meson Production and Chiral Dynamics*, April 8–9, 2005, Osaka Univ., Osaka, Japan.
- [79] C. Itzykson and J.-B. Zuber, “*Quantum Field Theory*”, (McGraw Hill, Singapore, 1985), p. 45.